Evidence for Strong HONO Emission from Fertilized Agricultural Fields and its Remarkable Impact on Regional O 3 Pollution in the Summer North China Plain

Chaoyang Xue, Can Ye, Chenglong Zhang, Valéry Catoire, Pengfei Liu, Rongrong Gu, Jingwei Zhang, Zhuobiao Ma, Xiaoxi Zhao, Wenqian Zhang, et al.

Evidence for strong HONO emission from fertilized agricultural fields and its remarkable impact on regional O_3 pollution in the summer North China Plain

Chaoyang Xue[1, 2, #], Can Ye[1, #, a], Chenglong Zhang[1, 3], Valéry Catoire[2], Pengfei Liu[1, 3], Rongrong Gu[7], Jingwei Zhang[6], Zhuobiao Ma[1], Xiaoxi Zhao[1], Wenqian Zhang[5], Yangang Ren[4], Gisèle Krysztofiak[2], Shengrui Tong[5], Likun Xue[7], Junling An[6], Maofa Ge[5], Abdelwahid Mellouki[4, 7], Yujing Mu[1, 3*]

[1] Research Centre for Eco-Environmental Sciences, Chinese Academy of Sciences, Beijing 100085, China

[2] Laboratoire de Physique et Chimie de l'Environnement et de l'Espace (LPC2E), CNRS–Université Orléans–CNES, 45071 Orléans Cedex 2, France

[3] Centre for Excellence in Regional Atmospheric Environment, Institute of Urban Environment, Chinese Academy of Sciences, Xiamen 361021, China

[4] Institut de Combustion Aérothermique, Réactivité et Environnement, Centre National de la Recherche Scientifique (ICARE-CNRS), Observatoire des Sciences de l'Univers en région Centre, CS 50060, 45071 cedex02, Orléans, France

[5] Institute of Chemistry, Chinese Academy of Sciences, Beijing 100190, China

[6] State Key Laboratory of Atmospheric Boundary Layer Physics and Atmospheric Chemistry (LAPC), Institute of Atmospheric Physics (IAP), Chinese Academy of Sciences, Beijing 100029, China

[7] Environmental Research Institute, Shandong University, Qingdao, Shandong 266237, China

[a] now at: State Key Joint Laboratory of Environmental Simulation and Pollution Control, College of Environmental Sciences and Engineering, Peking University, Beijing 100871, China

Correspondence to: yjmu@rcees.ac.cn

Abstract

Summertime HONO concentrations were synchronously measured at two (an agricultural and a non-agricultural) sites in the North China Plain (NCP). Daytime HONO (1.4±0.6 ppbv) and HONO/NO_2 ((12±8)%) over the agricultural field after fertilization were found to be remarkably higher than those before fertilization, implying strong HONO emission from the fertilized fields. Synchronous enhancements of HONO and O_3 after fertilization at both sites suggested that the emitted HONO accelerated the local and the regional O_3 pollution. HONO budget analysis further revealed that its emission was significantly enhanced after fertilization. Soil HONO emission flux and its uncertainty were estimated and discussed. The estimated emission flux exhibited a distinct diurnal variation with a noontime maximum. Net OH production rate from HONO photolysis greatly exceeded that from O_3 photolysis over the agricultural field, and their maximum ratio of 4.7 was obtained after fertilization. We provide field evidence that fertilized fields in the NCP act as a strong HONO source, which accelerates daytime photochemistry, leading to an increase of regional photo-oxidants such as O_3. Considering the severe O_3 pollution in the summer NCP and that the large area of the agricultural field is regularly treated with high fertilization amount in this region, HONO emission should be taken into account in the regional air quality deterioration.

Keywords: HONO, nitrogen fertilization, agricultural fields, emission flux, O_3

1. Introduction

It is generally accepted that the photolysis of nitrous acid (HONO) initiates photochemistry in early morning[1] and makes a significant contribution to hydroxyl radicals (OH) during the whole day[2–4]. The sources of HONO, however, are still not well understood. Besides the known sources such as direct emission from vehicle exhaust[5,6], the gas-phase reaction of NO+OH, (photo-enhanced) NO_2 heterogeneous reactions on surfaces[7,8], and other sources[9,10], laboratory studies recently found that soil could be a potential HONO source through abiotic or biotic formation[11–16] with emission fluxes up to 20-3000 ng-N m^{-2} s^{-1} and it was influenced by various factors such as soil nutrient, pH, and bacteria type (Table S1). However, such high HONO emission fluxes obtained in the laboratory studies were not supported by field flux measurements; that is, the flux obtained in the field measurements (Table S2) was generally much less than 60 ng-N m^{-2} s^{-1}, most of which, however, was related to other HONO formation paths rather than emission from the soil. For example, Zhou et al.[17] found upward HONO fluxes <2.7 ng-N m^{-2} s^{-1} at a forest site, which was attributed to the photolysis of leaf surface nitrate. Laufs et al.[18] measured soil HONO emission fluxes <2.3 ng-N m^{-2} s^{-1} at an agricultural site, and the photosensitized NO_2 heterogeneous reaction on the ground surface was suggested to be responsible for the flux. The large difference between HONO emission fluxes measured in the laboratory and over fields may be due to different soil characteristics and types/amounts of the applied nitrogen fertilizer, which needs further research work.

In the North China Plain (NCP), a large area of cultivated land (>0.2×10^6 km^2) is regularly treated with intensive chemical nitrogen fertilizers[19] and could constitute a potential HONO source. However, there were only a few atmospheric HONO measurements[20] over the agricultural fields in the rural NCP by now to recognize the possible HONO emission from fertilized fields and its impact. Liu et al.[20] have measured HONO at an agricultural site in the NCP and performed model tests on various HONO formation paths. They found that strong unknown HONO sources might be related to the fertilized fields, but did not provide sufficient evidence or specifically estimate soil HONO emissions. Besides, our previous studies[21,22], in which a twin open-top dynamic chamber (OTC) method was developed, provided the first direct soil HONO emission flux measurement and found that soil HONO emission could be enhanced by chemical nitrogen fertilizer. The impact on atmospheric HONO levels was yet not quantified. Herein, atmospheric HONO and related parameters were simultaneously measured at an agricultural site and a non-

agricultural site in June 2017. Based on the measurement, we then 1) provided evidence of HONO emission from the fertilized soil through the atmospheric HONO budget analysis at the agricultural site during different fertilization periods, 2) provided evidence of the regional impact of fertilization on air quality in the NCP through the comparison between the two sites, and 3) quantified the contribution of the enhanced HONO to the atmospheric oxidizing capacity during different periods.

2. Experimental

2.1 Sites and instrumentation

The Station of Rural Environmental Chinese Academy of Sciences (SRE-CAS), located in Dongbaituo village (38°42′N, 115°15′E), Hebei province-China, was used as the agricultural site (Figure S1). It is surrounded by agricultural fields with winter-wheat and summer-maize rotation.[22] During the campaign, one intensive fertilization event for planting summer maize, which happens every year, was performed (see details in Section 2.2). The non-agricultural site (37°46′N, 118°59′E), Yellow River Delta Ecology Research Station of Coastal Wetland (YelRD) in the NCP, is surrounded by wide-open lands with no significant anthropogenic emissions within 10 km (Figure S1). Even the non-agricultural site is ~15 km west of the sea, air mass during the measurement periods was mainly originated from the inner NCP, and no fertilization was conducted within 20 km around this site, leading to an excellent background site to verify the regional impact of agricultural fertilization.[23] At both sites, HONO was continuously measured online by the LOPAP technique (LOng Path Absorption Photometer, Model-03, QUMA GmbH, Germany)[24]. Other instruments used at the two stations are shown in Text S1 of the Supporting Information (SI).

2.2 The fertilization event

In the NCP region, fertilization is regularly conducted for planting summer-maize in June every year, and it happened during the present campaign. Regarding the large area of agricultural fields in the NCP, the regional fertilization event may last 1-2 weeks. In the present campaign, few fertilization processes for the fields within 3 km around our station started 1-2 days after we started the measurements on 7th June 2017; as a consequence, we recorded limited data without the influence of fertilization, but it may still be affected by the regional fertilization, making it hard to get observations completely without fertilization impact. Note that we have performed a week

measurement at the same site from 1st to 6th August 2016, which was more than 6 weeks after this year's fertilization (A6FP), and the impact of fertilization on soil HONO emission was expected to be less effective. HONO levels in this period were similar to the first day of the present campaign. HONO levels showed a significant increase after fertilization compared to the first day. Therefore, we consider the observation in the first day (with the smallest fertilization impact) as the representative for the rural background HONO levels during the non-fertilization period (NFP, see details in Text S2).

Most fertilization within 3 km around our station was conducted between 12th and 15th June 2017, and fields surrounding the station were fertilized on 13th June with an ammonium-based fertilization amount of ~180 kg-N ha^{-1}. We then classified the observations before 13th June as the pre-intensive fertilization period (PFP) and after 13th June as the intensive fertilization period (IFP). For comparison between the two sites, data at YelRD station was similarly classified into three periods (NFP: 1st-7th June 2017, PFP: 8th-13th June 2017, IFP: 14th-22nd June 2017).

3. Results

Figure S2 shows the time series of hourly average HONO, NO_2, O_3, H_2O_2, and solar irradiance (Ra) measured at the agricultural site during the four periods. During NFP, the averaged daytime (6:00-18:00) mixing ratios of HONO, NO_2, and O_3 were 0.36±0.26, 13.3±7.6, and 50±25 ppbv, respectively. Both daytime HONO and O_3 clearly showed significant increases during PFP (0.72±0.32 and 53±30 ppbv) and IFP (1.36±0.60 and 70±32 ppbv) in comparison with NFP (Table S3). Daytime H_2O_2 showed similar levels during NFP (0.66 ppbv) and PFP (0.60 ppbv), and a significant increase during IFP (0.95 ppbv). In contrast, there were no evident variations of NO_2 (an essential precursor for both HONO and O_3) and solar irradiance during the three periods (Table S3, Figure S2, and Figure S3).

Figure 1A exhibits the diurnal variations of HONO during the three periods (NFP, PFP, and IFP) at the agricultural site. During NFP, HONO showed a typical diurnal variation with high values during nighttime and noontime minimum. After fertilization, HONO mixing ratios increased significantly during PFP and IFP compared to NFP, and an unexpectedly high peak of 1.70 ppbv occurred at noontime (13:00) during IFP. In particular, the noontime HONO concentration during IFP was more than 2 times higher than that during PFP (0.71 ppbv) and more than 11 times greater than that during NFP (0.15 ppbv).

Figure 1B and 1C illustrate the diurnal variations of O_3 and H_2O_2 at the agricultural site. Both O_3 and H_2O_2 exhibited similar diurnal variations with peaks in the early afternoon and minima at night. However, O_3 and H_2O_2 in the morning (6:00-13:00) during IFP increased much faster than those during NFP or PFP, leading to higher noontime peaks of O_3 (103 ppbv) and H_2O_2 (1.98 ppbv). Besides, the occurrence time of peak O_3 during IFP (13:00) shifted >3 hours earlier than that during the other two periods (NFP: 16:00, PFP: 17:00). It approached the occurrence time (13:00) of the high daytime HONO peak when OH production from HONO photolysis is the largest in a day, indicating the possible influence of elevated HONO on O_3 formation after the intensive fertilization.

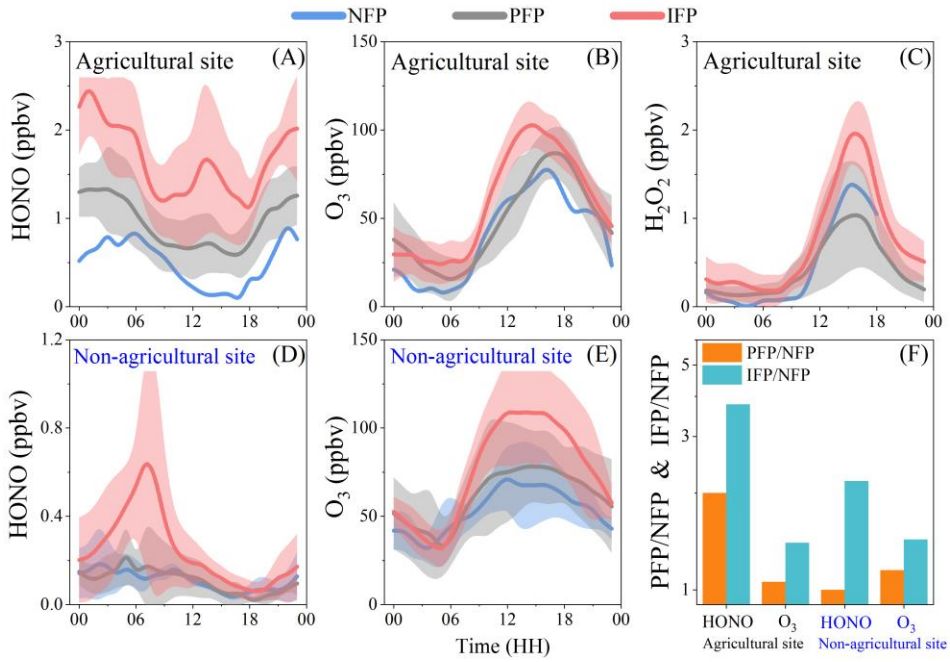

Figure 1 Diurnal variations of HONO (A), O_3 (B), and H_2O_2 (C) during the three periods at the agricultural site, HONO (D) and O_3 (E) during the three periods (non-fertilization period: NFP in blue, pre-intensive fertilization period: PFP in grey, intensive fertilization period: IFP in red) at the non-agricultural site, and the daytime enhancement factor of HONO or O_3 during PFP and IFP compared to NFP (F). The error bars represent the standard deviations (±1σ).

Figure 1D and 1E show diurnal variations of HONO and O_3 at the non-agricultural site, respectively. HONO mixing ratios were generally lower than 1 ppbv, similar to those during NFP at the agricultural site. Evident enhancement of HONO with a small noontime peak was also observed during IFP compared to NFP or PFP at the non-agricultural site. Similar to the

agricultural site, O_3 at the non-agricultural site showed a small increase during PFP but an evident increase during IFP with respect to NFP.

The enhancement factors (EF, defined as average daytime mixing ratio of one specific pollutant during PFP or IFP divided by that during NFP) for HONO and O_3 at the two sites are shown in Figure 1F. EF values for HONO or O_3 at the agricultural site were much larger than those at the non-agricultural site, and all the EFs were larger than 1, implying that both HONO and O_3 at the two sites were enhanced during PFP and IFP. Due to the significant daytime increase of HONO and O_3, the EFs for HONO and O_3 during IFP at the agricultural site reached 3.8 and 2.0, respectively. Note that EF for HONO at noontime was even larger. For example, noontime average HONO during IFP was more than one order of magnitude higher than that during NFP (EF>10).

4. Discussion

4.1 HONO budget

At noontime in summer, the photolytic loss of HONO is usually very rapid, e.g., the photolytic lifetime of HONO (1/J(HONO)) was <15 min at noontime during this campaign, and thus, its source strength is expected to be nearly equal to its sink strength.[25,26] HONO formation from homogeneous reaction NO+OH (P_{NO+OH}) and photo-enhanced NO_2 uptake on the ground surface (P_{het}) could be calculated. Then, HONO formation from the unknown sources ($P_{unknown}$) was calculated in Text S4.

Figure S4 shows the average daytime HONO formation rate from each pathway during the three periods at the agricultural site. HONO formation during NFP was dominated by P_{NO+OH} and P_{het} with a sum contribution of 97%, leading to a small contribution (3%) from $P_{unknown}$. However, $P_{unknown}$ remarkably exceeded P_{NO+OH} and P_{het} during PFP and IFP with contributions of 63% and 81%, respectively. It is evident that HONO formation from unknown sources significantly increased after fertilization (during PFP and IFP).

The key question is which source made a dominant contribution to $P_{unknown}$ during PFP and IFP. A recent study[20] revealed that vehicle emission, NO_2 reaction on the aerosol surface, NO_2 reaction on soot surface, acid displacement, photolysis of nitrophenol, and biomass burning had negligible impacts on the daytime HONO formation at this site. And Liu et al. proposed that soil emission and total nitrate (TNO_3=HNO_3+pNO_3) photolysis might be the potential HONO sources that account for unexpectedly high daytime HONO levels. Assuming a high TNO_3 concentration of 12

ppbv observed at this site in summer 2014[20], a high photolysis frequency of 1×10^{-5} s^{-1} (~2 orders of magnitude higher than HNO_3(g) photolysis[27–29], and a maximum HONO yield of 100%, HONO production rate from TNO_3 photolysis was about 0.4 ppbv h^{-1}, which is far to explain $P_{unknown}$ during PFP (1.6±1.0 ppbv h^{-1}) and IFP (4.3±2.0ppbv h^{-1}). Therefore, the other source, soil emission from the fertilized field, was suspected to be responsible for the extremely high $P_{unknown}$ (also discussed in the following section).

4.2 Evidence for soil HONO emission: HONO/NO_2

Firstly, as discussed before, $P_{unknown}$ and its contribution to daytime HONO formation showed a significant increase after fertilization (Figure 2B and Figure S4), implying the potential HONO enhancement caused by fertilization.

Secondly, photo-enhanced heterogeneous reactions of NO_2 on ground surfaces have been considered as important daytime HONO sources[7,8,18], which could be verified by the P_{het} obtained by the present study during non-fertilization periods in summer (Figure S4) as well as by our previous investigation in winter[30]. Thus, the HONO/NO_2 ratio was used to evaluate the role of NO_2-relevant reactions in HONO formation. As shown in Figure 2A and Table S3, the average HONO/NO_2 during A6FP and NFP was (2.1±1.2)% and (2.6±1.0)%, respectively, comparable to previous observations (1%-5%) without significant impact from soil emission[3,18,31–33], indicating the important role of NO_2 reactions in HONO formation before fertilization and 6 weeks after fertilization. However, the significantly higher HONO/NO_2 ratios during PFP (mean: (5.4±3.7)%, maximum: 22%) and IFP (mean: (11.8±8.0)%, maximum: 38%) could not be explained by NO_2-relevant reactions with respect to the comparable NO_2 mixing ratios during the three periods (Figure S3 and Table S3). Note that the HONO/NO_2 used here are expected even larger if NO_2 is furtherly corrected by HNO_3, etc. (See Text S1). In particular, the maximum HONO/NO_2 ratio after fertilization reached 38% (Table S3), which dramatically exceeds the values mainly dominated by NO_2-relevant reactions.[3,18,31,32]

Taken together, the remarkable increase of atmospheric HONO levels and the extremely high HONO/NO_2 ratios, as well as $P_{unknown}$ during IFP, were reasonably attributed to HONO emission from the fertilized field, which is in agreement with the results of our previous field flux studies at this site, in which we found strong HONO emissions (especially around noontime) from the fertilized soil in summer 2016[21,22].

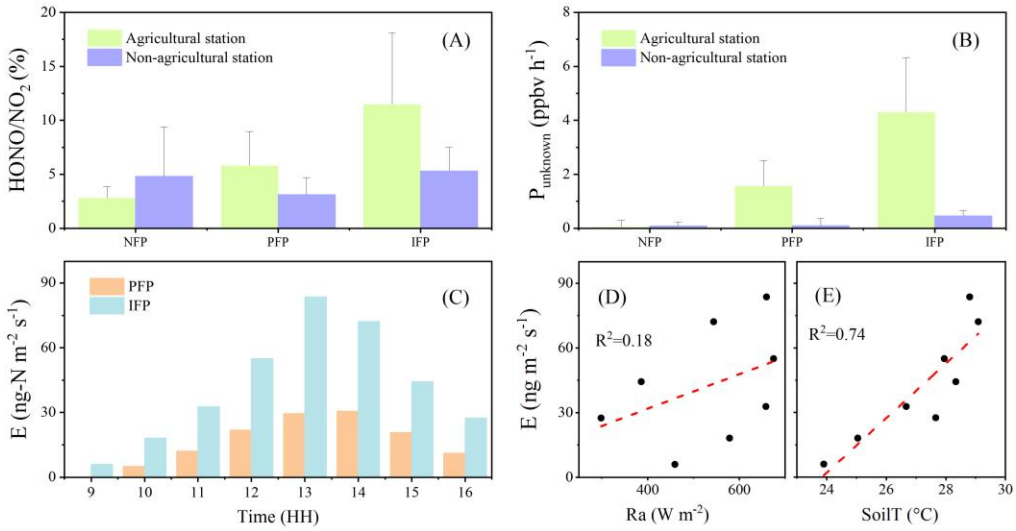

Figure 2 (A) & (B): HONO/NO_2 or $P_{unknown}$ during NFP, PFP, and IFP at the two stations; (C): The inferred HONO emission flux based on MLH*0.35 during PFP and IFP. (D) & (E): Correlations of E with solar radiation or soil temperature.

4.3 Soil HONO emission flux estimation and discussion on the mechanism

The increase of $P_{unknown}$ during PFP and IFP in comparison with NFP was mainly attributed to the HONO emission from the fertilized field. Thus, the soil HONO emission flux (E, in ng-N m^{-2} s^{-1}) was estimated based on the enhanced $P_{unknown}$ and the mixing layer height (MLH), as shown in Text S5. However, vertical distribution of HONO is expected when a ground-based source is dominated, leading to an overestimated emission flux when using the ground measurement (3.4 m above the ground) as the average HONO within the calculated MLH. The maximum value and the variation trend of MLH can be scaled by the turbulence and the boundary layer height (BLH), respectively (see Text S5 and Figure S5), but this results in an overestimated MLH because HONO decreases to 1/e (37%) within its lifetime. Hence, we furtherly analyzed the HONO budget during NFP when daytime HONO formation was dominated by photo-enhanced NO_2 uptake on the ground surface. A more reasonable MLH could be achieved when HONO formation could be nearly fully explained by NO+OH and the photo-enhanced NO_2 uptake on the ground surface. We found that when MLH*0.35 (maximum: 70 m at noontime) was used in $P(HONO)_{het}$ calculation, almost all the HONO formation (97%) could be explained by NO+OH and the photo-enhanced NO_2 uptake on the ground surface, revealing that MLH*0.35 is reasonable to represent the mixing layer height when ground sources dominate HONO formation. Because both soil emission and the

photo-enhanced NO_2 reaction happen on the ground surface, MLH*0.35 is also valid for soil HONO emission flux calculation.

Figure 2C shows the inferred E during PFP and IFP. Both the emission fluxes during PFP and IFP exhibit a distinct diurnal variation, with a noontime peak. Maximum E during IFP is 84 ng-N m^{-2} s^{-1}, which is comparable to those from our field flux measurement from ammonium-fertilized soils[22], but higher than those measured in other places with upward fluxes less than (generally much less than) 60 ng-N m^{-2} s^{-1} (Table S2). The inferred emission flux is also lower than most of the high values obtained from the laboratory studies (Table S1). Nevertheless, it should be noted that the evidence of soil HONO emission enhanced by the agricultural nitrogen fertilization is consistent with our previous direct flux measurements. Still, the estimation of soil HONO emission flux is of some uncertainties; for example, the uncertainty caused by the estimated MLH as discussed before. Therefore, further direct flux measurement is necessary to quantify the emission flux and its regional impact accurately.

In the NCP, agricultural fields were treated with long-term and high amounts of ammonium- or urea-based chemical nitrogen fertilizers, which has been expected to accelerate nitrification significantly.[13,34–37] Nitrite (NO_2^-) is the key intermediate product of ammonium nitrification and could lead to HONO formation through coupling with a hydrogen ion. Although the agricultural soils in the NCP are slightly alkaline (the measured pH is ~8), which is not in favor of HONO formation based on the acid-based equilibrium[11], the micro-environment, for example, at the nitrifying bacteria level, is expected to be different from the bulk condition because of the release of hydrogen ions from the nitrification[37,38] as well as the surface water loss[11,13], which may influence surface/microscale pH.[12,39] It should also be noted that the strong HONO emission from the fertilized agricultural field during IFP occurred under the condition with the measured soil water content greater than 80% of the water holding capacity (WHC) due to the flooding irrigation after fertilization, and it is not consistent with laboratory results that high emission occurred at 10%-30% WHC (obtained from dry air flushed flow tube experiments)[13,40]. HONO is soluble easily under high soil water content (e.g., 80% WHC for bulk soil within 5 cm depth). The water content of the soil surface is, however, expected to be lower than the bulk one because of water evaporation that is in favor of HONO emission, indicating the key role of microscale parameters (e.g., on the soil surface) in soil HONO emission.[12,39] Besides, HONO might be emitted by bacteria under high soil water content, i.e., HONO could be emitted under (75%-140%)WHC reported by

Wu et al.[16] We then support that NO_2^- is produced by soil bacteria under a proper water content and the surface process governs the transmission of NO_2^- (ag) to gas-phase HONO. Further studies focused on the link of changes in the microenvironment with reactive nitrogen emission are still of significant importance.

Besides, the correlation of E with soil temperature (R^2=0.74) is much higher than that with solar radiation (R^2=0.17) (Figure 2D and 2F), suggesting the critical role of soil temperature in soil HONO emission, e.g., soil temperature could largely influence the biogenic process (e.g., nitrification[13,40,41]) and enhance surface water evaporation.[11–13,39]

5 Atmospheric implications on the atmospheric oxidizing capacity and O_3 pollution in the NCP

The remarkable increase of atmospheric HONO due to soil emission could accelerate OH formation through its photolysis (see detailed OH production rate calculation in Text S6). Figure 3 shows the OH production rates from the photolysis of HONO ($P(OH)_{HONO}$) and O_3 ($P(OH)_{O_3}$). $P(OH)_{HONO}$ quickly increased from early morning to around noontime, whereas $P(OH)_{O_3}$ started to rise 2 hours later. Daytime $P(OH)_{O_3}$ was generally lower than $P(OH)_{HONO}$ during NFP and much lower during PFP and IFP, implying the predominant role of HONO in OH production. Compared to NFP (or PFP), daytime average $P(OH)_{HONO}$ increased from 0.8±0.5 (or 1.5±1.2) to 3.0±2.1 ppbv h^{-1}, while $P(OH)_{O_3}$ kept at a low level (mean <0.7 ppbv h^{-1}). The largest $P(OH)_{HONO}$ reached 10.7 ppbv h^{-1} at 13:00 on 18th June when HONO reached as high as 3.1 ppbv under high solar irradiance expressed as $J(NO_2)=6.2\times10^{-3}$ s^{-1}. To the best of our knowledge, such a high OH production rate from HONO photolysis, is the largest one found in rural sites, including (fertilized) agricultural sites[18,20,25,30], forest sites[2,17], grass sites[42–44], or other rural sites[23,28], suggesting the crucial role of soil HONO emission in the atmospheric oxidizing capacity in this region.

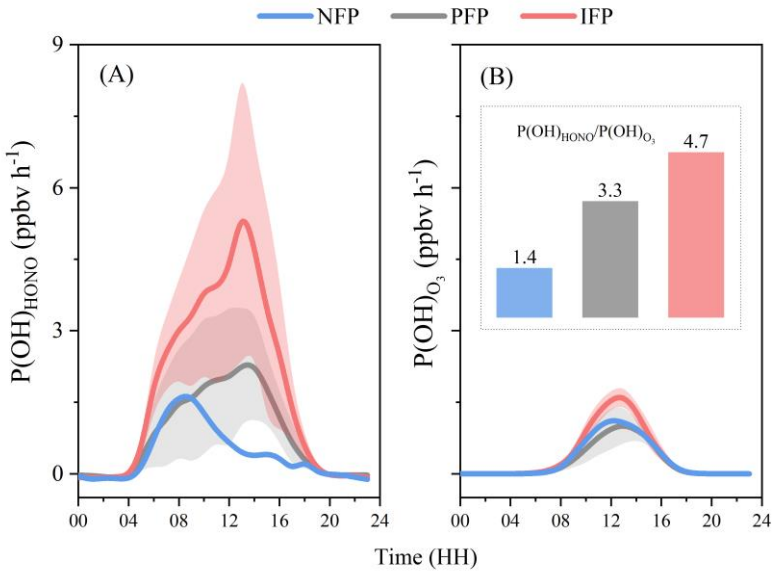

Figure 3 The average diurnal variations of the net OH production rates from photolysis of HONO (A) and O_3 (B) during the three periods. The shadowed areas represent the standard deviations (±1σ). The average ratio of $P(OH)_{HONO}$ to $P(OH)_{O_3}$ was also shown as a column plot (B).

The evident rises of O_3 and H_2O_2 (Figure 1B and 1C) after fertilization could be attributed to the remarkable increase of $P(OH)_{HONO}$ that dominates the enhanced OH production, which could consequently promote the production of O_3 and H_2O_2 through reactions (1)-(5):

$$OH + VOCs/CO \xrightarrow{O_2} HO_2/RO_2 \quad (1)$$

$$HO_2/RO_2 + NO \rightarrow NO_2 + OH/RO \quad (2)$$

$$NO_2 + h\nu \rightarrow NO + O(^3P) \quad (3)$$

$$O(^3P) + O_2 + M \rightarrow O_3 + M\ (M = N_2/O_2) \quad (4)$$

$$HO_2 + HO_2 + (M) \rightarrow H_2O_2 + (M) \quad (5)$$

It is worth noting that both the largest enhancements of O_3 (Figure 1B) and $P(OH)_{HONO}$ (Figure 3A) from PFP to IFP occurred at the same time of 13:00, in concert with the maximum emission flux (Figure 2C). Meanwhile, a recent WRF-Chem model study[45] and our box model study[30] also showed that additional HONO sources significantly impacted HO_x and O_3 concentrations, consistent with our conclusion.

Additionally, the emitted HONO may also influence regional HONO and O_3 levels, e.g., the significant increase of HONO, O_3, and $P_{unknown}$ values during IFP at the non-agricultural site (Figure 1Figure 2) resulted from the air mass from the inner NCP during IFP (Figures S6 and S7). Because the HONO level at the non-agricultural site is much lower than that at the agricultural site,

the impact on the non-agricultural site could be very significant even if only a small part of HONO emitted by the agricultural field reached the non-agricultural site. On the one hand, enhanced regional OH levels caused by the elevated HONO could accelerate NO+OH reaction; on the other hand, high wind speeds (e.g., 9 m s^{-1} from the inner NCP) observed at the non-agricultural site may also enable a rapid air mass transport from the agricultural fields to the non-agricultural site. As is expected, high HONO, O_3, and HONO/NO_2 levels were also frequently observed in the airmass originated from the inner NCP (Figure S7), demonstrating the potential regional impact of fertilization on the air quality of the whole NCP.

Given that the maize planting with intensive fertilization (96-482 kg-N ha^{-1}) is regularly conducted every June in the NCP[19], soil HONO emission is suspected to occur in most agricultural fields (>0.2×10^6 km^2) because the soil characters and meteorological conditions are quite similar in this region[41]. Thus, the significant elevation of atmospheric oxidants (i.e., O_3 and H_2O_2) could also be expected in the whole NCP region after fertilization for planting summer maize, and it can be furtherly confirmed by the synchronous enhancements of O_3 concentrations during IFP at the agricultural site and the non-agricultural site. Therefore, the impact of HONO emission from the agricultural fields on regional atmospheric oxidants is necessary to be quantitatively evaluated by further long-term field measurements along with direct OH measurement and model simulations, and it is, as well, essential for disclosing the reasons for the severe O_3 pollution in the summer NCP and similar regions.[46,47]

Acknowledgments

We are grateful to Liwei Guan for his contribution to the field measurements. We thank Yunqiao Zhou for his help with map plotting. **Funding:** This work was supported by the National Natural Science Foundation of China (No. 91544211, 41727805, 41931287, 41975164). **Author contribution:** Y.M. led the study. C.X., C.Z., P.L., C.Y., Z.M., W.Z., S.T., and X.Z. performed measurements at SRE-CAS station. R.G. and L.X. provided and analyzed field data at YelRD station. C.Y., J.Z., Y.R., M.G., and J.A. made discussions on data analysis and writing process. C.X. and Y.M. wrote this manuscript with all the authors' contributions. V.C., G.K., L.X., and A.M. provided scientific advice on the study and revised this manuscript. # C.X. and C.Y. contributed equally. **Competing interests:** The authors declare no competing financial interest.

Data availability: Observation data used in this study can be requested from the corresponding author.

Supporting Information Available

A description of instruments used in this campaign (Text S1), HONO levels during the non-fertilization period (Text S2), J values calculation method (Text S3), $P_{unknown}$ calculation (Text S4), HONO emission flux calculation (Text S5), net OH production rate calculation (Text S6), 7 additional figures, and 3 additional tables.

References

(1) Alicke, B.; Geyer, A.; Hofzumahaus, A.; Holland, F.; Konrad, S.; Pätz, H. W.; Schäfer, J.; Stutz, J.; Volz-Thomas, A.; Platt, U. OH Formation by HONO Photolysis during the BERLIOZ Experiment. *J. Geophys. Res. Atmos.* **2003**, *108* (4), 3–1. https://doi.org/10.1029/2001jd000579.

(2) Kleffmann, J.; Gavriloaiei, T.; Hofzumahaus, A.; Holland, F.; Koppmann, R.; Rupp, L.; Schlosser, E.; Siese, M.; Wahner, A. Daytime Formation of Nitrous Acid: A Major Source of OH Radicals in a Forest. *Geophys. Res. Lett.* **2005**, *32* (5), L05818. https://doi.org/10.1029/2005GL022524.

(3) Kim, S.; VandenBoer, T. C.; Young, C. J.; Riedel, T. P.; Thornton, J. A.; Swarthout, B.; Sive, B.; Lerner, B.; Gilman, J. B.; Warneke, C.; Roberts, J. M.; Guenther, A.; Wagner, N. L.; Dubé, W. P.; Williams, E.; Brown, S. S. The Primary and Recycling Sources of OH during the NACHTT-2011 Campaign: HONO as an Important OH Primary Source in the Wintertime. *J. Geophys. Res. Atmos.* **2014**, *119* (11), 6886–6896. https://doi.org/10.1002/2013JD019784.

(4) Tan, Z.; Fuchs, H.; Lu, K.; Hofzumahaus, A.; Bohn, B.; Broch, S.; Dong, H.; Gomm, S.; Häseler, R.; He, L.; Holland, F.; Li, X.; Liu, Y.; Lu, S.; Rohrer, F.; Shao, M.; Wang, B.; Wang, M.; Wu, Y.; Zeng, L.; Zhang, Y.; Wahner, A.; Zhang, Y. Radical Chemistry at a Rural Site (Wangdu) in the North China Plain: Observation and Model Calculations of OH, HO_2 and RO_2 Radicals. *Atmos. Chem. Phys.* **2017**, *17* (1), 663–690. https://doi.org/10.5194/acp-17-663-2017.

(5) Kurtenbach, R.; Becker, K. H.; Gomes, J. A. G.; Kleffmann, J.; Lörzer, J. C.; Spittler, M.; Wiesen, P.; Ackermann, R.; Geyer, A.; Platt, U. Investigations of Emissions and

Heterogeneous Formation of HONO in a Road Traffic Tunnel. *Atmos. Environ.* **2001**, *35* (20), 3385–3394. https://doi.org/10.1016/S1352-2310(01)00138-8.

(6) Liu, Y.; Lu, K.; Ma, Y.; Yang, X.; Zhang, W.; Wu, Y.; Peng, J.; Shuai, S.; Hu, M.; Zhang, Y. Direct Emission of Nitrous Acid (HONO) from Gasoline Cars in China Determined by Vehicle Chassis Dynamometer Experiments. *Atmos. Environ.* **2017**, *169*, 89–96. https://doi.org/10.1016/j.atmosenv.2017.07.019.

(7) George, C.; Strekowski, R. S.; Kleffmann, J.; Stemmler, K.; Ammann, M. Photoenhanced Uptake of Gaseous NO_2 on Solid Organic Compounds: A Photochemical Source of HONO? *Faraday Discuss.* **2005**, *130*, 195–210. https://doi.org/10.1039/b417888m.

(8) Stemmler, K.; Ammann, M.; Donders, C.; Kleffmann, J.; George, C. Photosensitized Reduction of Nitrogen Dioxide on Humic Acid as a Source of Nitrous Acid. *Nature* **2006**, *440* (7081), 195–198. https://doi.org/10.1038/nature04603.

(9) Bejan, I.; Abd El Aal, Y.; Barnes, I.; Benter, T.; Bohn, B.; Wiesen, P.; Kleffmann, J. The Photolysis of Ortho-Nitrophenols: A New Gas Phase Source of HONO. *Phys. Chem. Chem. Phys.* **2006**, *8* (17), 2028–2035. https://doi.org/10.1039/b516590c.

(10) Vandenboer, T. C.; Young, C. J.; Talukdar, R. K.; Markovic, M. Z.; Brown, S. S.; Roberts, J. M.; Murphy, J. G. Nocturnal Loss and Daytime Source of Nitrous Acid through Reactive Uptake and Displacement. *Nat. Geosci.* **2015**, *8* (1), 55–60. https://doi.org/10.1038/ngeo2298.

(11) Su, H.; Cheng, Y.; Oswald, R.; Behrendt, T.; Trebs, I.; Meixner, F. X.; Andreae, M. O.; Cheng, P.; Zhang, Y.; Pöschl, U. Soil Nitrite as a Source of Atmospheric HONO and OH Radicals. *Science* **2011**, *333* (6049), 1616–1618. https://doi.org/10.1126/science.1207687.

(12) Donaldson, M. A.; Bish, D. L.; Raff, J. D. Soil Surface Acidity Plays a Determining Role in the Atmospheric-Terrestrial Exchange of Nitrous Acid. *Proc. Natl. Acad. Sci. U. S. A.* **2014**, *111* (52), 18472–18477. https://doi.org/10.1073/pnas.1418545112.

(13) Scharko, N. K.; Schütte, U. M. E.; Berke, A. E.; Banina, L.; Peel, H. R.; Donaldson, M. A.; Hemmerich, C.; White, J. R.; Raff, J. D. Combined Flux Chamber and Genomics Approach Links Nitrous Acid Emissions to Ammonia Oxidizing Bacteria and Archaea in Urban and Agricultural Soil. *Environ. Sci. Technol.* **2015**, *49* (23), 13825–13834. https://doi.org/10.1021/acs.est.5b00838.

(14) Weber, B.; Wu, D.; Tamm, A.; Ruckteschler, N.; Rodríguez-Caballero, E.; Steinkamp, J.;

Meusel, H.; Elbert, W.; Behrendt, T.; Sörgel, M.; Cheng, Y.; Crutzen, P. J.; Su, H.; Pöschl, U. Biological Soil Crusts Accelerate the Nitrogen Cycle through Large NO and HONO Emissions in Drylands. *Proc. Natl. Acad. Sci.* **2015**, *112* (50), 15384–15389. https://doi.org/10.1073/pnas.1515818112.

(15) Ermel, M.; Behrendt, T.; Oswald, R.; Derstroff, B.; Wu, D.; Hohlmann, S.; Stönner, C.; Pommerening-Röser, A.; Könneke, M.; Williams, J.; Meixner, F. X.; Andreae, M. O.; Trebs, I.; Sörgel, M. Hydroxylamine Released by Nitrifying Microorganisms Is a Precursor for HONO Emission from Drying Soils. *Sci. Rep.* **2018**, *8* (1), 1877. https://doi.org/10.1038/s41598-018-20170-1.

(16) Wu, D.; Horn, M. A.; Behrendt, T.; Müller, S.; Li, J.; Cole, J. A.; Xie, B.; Ju, X.; Li, G.; Ermel, M.; Oswald, R.; Fröhlich-Nowoisky, J.; Hoor, P.; Hu, C.; Liu, M.; Andreae, M. O.; Pöschl, U.; Cheng, Y.; Su, H.; Trebs, I.; Weber, B.; Sörgel, M. Soil HONO Emissions at High Moisture Content Are Driven by Microbial Nitrate Reduction to Nitrite: Tackling the HONO Puzzle. *ISME J.* **2019**, *13* (7), 1688–1699. https://doi.org/10.1038/s41396-019-0379-y.

(17) Zhou, X.; Zhang, N.; TerAvest, M.; Tang, D.; Hou, J.; Bertman, S.; Alaghmand, M.; Shepson, P. B.; Carroll, M. A.; Griffith, S.; Dusanter, S.; Stevens, P. S. Nitric Acid Photolysis on Forest Canopy Surface as a Source for Tropospheric Nitrous Acid. *Nat. Geosci.* **2011**, *4* (7), 440–443. https://doi.org/10.1038/ngeo1164.

(18) Laufs, S.; Cazaunau, M.; Stella, P.; Kurtenbach, R.; Cellier, P.; Mellouki, A.; Loubet, B.; Kleffmann, J. Diurnal Fluxes of HONO above a Crop Rotation. *Atmos. Chem. Phys.* **2017**, *17* (11), 6907–6923. https://doi.org/10.5194/acp-17-6907-2017.

(19) Miao, Y.; Stewart, B. A.; Zhang, F. Long-Term Experiments for Sustainable Nutrient Management in China. A Review. *Agron. Sustain. Dev.* **2011**, *31* (2), 397–414. https://doi.org/10.1051/agro/2010034.

(20) Liu, Y.; Lu, K.; Li, X.; Dong, H.; Tan, Z.; Wang, H.; Zou, Q.; Wu, Y.; Zeng, L.; Hu, M.; Min, K. E.; Kecorius, S.; Wiedensohler, A.; Zhang, Y. A Comprehensive Model Test of the HONO Sources Constrained to Field Measurements at Rural North China Plain. *Environ. Sci. Technol.* **2019**, *53* (7), 3517–3525. https://doi.org/10.1021/acs.est.8b06367.

(21) Tang, K.; Qin, M.; Duan, J.; Fang, W.; Meng, F.; Liang, S.; Xie, P.; Liu, J.; Liu, W.; Xue, C.; Mu, Y. A Dual Dynamic Chamber System Based on IBBCEAS for Measuring Fluxes

of Nitrous Acid in Agricultural Fields in the North China Plain. *Atmos. Environ.* **2019**, *196*, 10–19. https://doi.org/10.1016/j.atmosenv.2018.09.059.

(22) Xue, C.; Ye, C.; Zhang, Y.; Ma, Z.; Liu, P.; Zhang, C.; Zhao, X.; Liu, J.; Mu, Y. Development and Application of a Twin Open-Top Chambers Method to Measure Soil HONO Emission in the North China Plain. *Sci. Total Environ.* **2019**, *659*, 621–631. https://doi.org/10.1016/j.scitotenv.2018.12.245.

(23) Gu, R.; Zheng, P.; Chen, T.; Dong, C.; Wang, Y.; Liu, Y.; Liu, Y.; Luo, Y.; Han, G.; Wang, X.; Zhou, X.; Wang, T.; Wang, W.; Xue, L. Atmospheric Nitrous Acid (HONO) at a Rural Coastal Site in North China: Seasonal Variations and Effects of Biomass Burning. *Atmos. Environ.* **2020**, *229*, 117429. https://doi.org/10.1016/j.atmosenv.2020.117429.

(24) Heland, J.; Kleffmann, J.; Kurtenbach, R.; Wiesen, P. A New Instrument To Measure Gaseous Nitrous Acid (HONO) in the Atmosphere. *Environ. Sci. Technol.* **2001**, *35* (15), 3207–3212. https://doi.org/10.1021/es000303t.

(25) Ren, X.; Sanders, J. E.; Rajendran, A.; Weber, R. J.; Goldstein, A. H.; Pusede, S. E.; Browne, E. C.; Min, K. E.; Cohen, R. C. A Relaxed Eddy Accumulation System for Measuring Vertical Fluxes of Nitrous Acid. *Atmos. Meas. Tech.* **2011**, *4* (10), 2093–2103. https://doi.org/10.5194/amt-4-2093-2011.

(26) Pusede, S. E.; VandenBoer, T. C.; Murphy, J. G.; Markovic, M. Z.; Young, C. J.; Veres, P. R.; Roberts, J. M.; Washenfelder, R. A.; Brown, S. S.; Ren, X.; Tsai, C.; Stutz, J.; Brune, W. H.; Browne, E. C.; Wooldridge, P. J.; Graham, A. R.; Weber, R.; Goldstein, A. H.; Dusanter, S.; Griffith, S. M.; Stevens, P. S.; Lefer, B. L.; Cohen, R. C. An Atmospheric Constraint on the NO_2 Dependence of Daytime Near-Surface Nitrous Acid (HONO). *Environ. Sci. Technol.* **2015**, *49* (21), 12774–12781. https://doi.org/10.1021/acs.est.5b02511.

(27) Laufs, S.; Kleffmann, J. Investigations on HONO Formation from Photolysis of Adsorbed HNO_3 on Quartz Glass Surfaces. *Phys. Chem. Chem. Phys.* **2016**, *18* (14), 9616–9625. https://doi.org/10.1039/C6CP00436A.

(28) Romer, P. S.; Wooldridge, P. J.; Crounse, J. D.; Kim, M. J.; Wennberg, P. O.; Dibb, J. E.; Scheuer, E.; Blake, D. R.; Meinardi, S.; Brosius, A. L.; Thames, A. B.; Miller, D. O.; Brune, W. H.; Hall, S. R.; Ryerson, T. B.; Cohen, R. C. Constraints on Aerosol Nitrate Photolysis as a Potential Source of HONO and NO_X. *Environ. Sci. Technol.* **2018**, *52* (23), 13738–

13746. https://doi.org/10.1021/acs.est.8b03861.

(29) Bao, F.; Li, M.; Zhang, Y.; Chen, C.; Zhao, J. Photochemical Aging of Beijing Urban $PM_{2.5}$: HONO Production. *Environ. Sci. Technol.* **2018**, *52* (11), 6309–6316. https://doi.org/10.1021/acs.est.8b00538.

(30) Xue, C.; Zhang, C.; Ye, C.; Liu, P.; Catoire, V.; Krysztofiak, G.; Chen, H.; Ren, Y.; Zhao, X.; Wang, J.; Zhang, F.; Zhang, C.; Zhang, J.; An, J.; Wang, T.; Chen, J.; Kleffmann, J.; Mellouki, A.; Mu, Y. HONO Budget and Its Role in Nitrate Formation in the Rural North China Plain. *Environ. Sci. Technol.* **2020**, *54* (18), 11048–11057. https://doi.org/10.1021/acs.est.0c01832.

(31) Kleffmann, J.; Kurtenbach, R.; Lörzer, J.; Wiesen, P.; Kalthoff, N.; Vogel, B.; Vogel, H. Measured and Simulated Vertical Profiles of Nitrous Acid - Part I: Field Measurements. *Atmos. Environ.* **2003**, *37* (21), 2949–2955. https://doi.org/10.1016/S1352-2310(03)00242-5.

(32) Wong, K. W.; Oh, H.-J.; Lefer, B. L.; Rappenglück, B.; Stutz, J. Vertical Profiles of Nitrous Acid in the Nocturnal Urban Atmosphere of Houston, TX. *Atmos. Chem. Phys.* **2011**, *11* (8), 3595–3609. https://doi.org/10.5194/acp-11-3595-2011.

(33) Stutz, J.; Alicke, B.; Ackermann, R.; Geyer, A.; Wang, S.; White, A. B.; Williams, E. J.; Spicer, C. W.; Fast, J. D. Relative Humidity Dependence of HONO Chemistry in Urban Areas. *J. Geophys. Res. Atmos.* **2004**, *109*, D03307. https://doi.org/10.1029/2003JD004135.

(34) Ye, C.; Liu, P.; Ma, Z.; Xue, C.; Zhang, C.; Zhang, Y.; Liu, J.; Liu, C.; Sun, X.; Mu, Y. High H_2O_2 Concentrations Observed during Haze Periods during the Winter in Beijing: Importance of H_2O_2 Oxidation in Sulfate Formation. *Environ. Sci. Technol. Lett.* **2018**, *5* (12), 757–763. https://doi.org/10.1021/acs.estlett.8b00579.

(35) Akiyama, H.; Morimoto, S.; Hayatsu, M.; Hayakawa, A.; Sudo, S.; Yagi, K. Nitrification, Ammonia-Oxidizing Communities, and N_2O and CH_4 Fluxes in an Imperfectly Drained Agricultural Field Fertilized with Coated Urea with and without Dicyandiamide. *Biol. Fertil. Soils* **2013**, *49* (2), 213–223. https://doi.org/10.1007/s00374-012-0713-2.

(36) Wang, F.; Chen, S.; Wang, Y.; Zhang, Y.; Hu, C.; Liu, B. Long-Term Nitrogen Fertilization Elevates the Activity and Abundance of Nitrifying and Denitrifying Microbial Communities in an Upland Soil: Implications for Nitrogen Loss From Intensive Agricultural Systems. *Front. Microbiol.* **2018**, *9* (OCT), 2424. https://doi.org/10.3389/fmicb.2018.02424.

(37) Guo, J. H.; Liu, X. J.; Zhang, Y.; Shen, J. L.; Han, W. X.; Zhang, W. F.; Christie, P.; Goulding, K. W. T.; Vitousek, P. M.; Zhang, F. S. Significant Acidification in Major Chinese Croplands. *Science* **2010**, *327* (5968), 1008–1010. https://doi.org/10.1126/science.1182570.

(38) Wrage, N.; Velthof, G. L.; Beusichem, M. L. Van; Oenema, O. Role of Nitrifier Denitrication in the Production of Nitrous Oxide. *Soil Biol. Biochem.* **2001**, *33* (12), 1723–1732. https://doi.org/10.1016/S0038-0717(01)00096-7.

(39) Kim, M.; Or, D. Microscale PH Variations during Drying of Soils and Desert Biocrusts Affect HONO and NH_3 Emissions. *Nat. Commun.* **2019**, *10* (1), 3944. https://doi.org/10.1038/s41467-019-11956-6.

(40) Oswald, R.; Behrendt, T.; Ermel, M.; Wu, D.; Su, H.; Cheng, Y.; Breuninger, C.; Moravek, A.; Mougin, E.; Delon, C.; Loubet, B.; Pommerening-Röser, A.; Sörgel, M.; Pöschl, U.; Hoffmann, T.; Andreae, M. O.; Meixner, F. X.; Trebs, I. HONO Emissions from Soil Bacteria as a Major Source of Atmospheric Reactive Nitrogen. *Science* **2013**, *341* (6151), 1233–1235. https://doi.org/10.1126/science.1242266.

(41) Zhang, Y.; Mu, Y.; Zhou, Y.; Tian, D.; Liu, J.; Zhang, C. NO and N_2O Emissions from Agricultural Fields in the North China Plain: Origination and Mitigation. *Sci. Total Environ.* **2016**, *551–552*, 197–204. https://doi.org/10.1016/j.scitotenv.2016.01.209.

(42) Harrison, R. M.; Kitto, A.-M. N. Evidence for a Surface Source of Atmospheric Nitrous Acid. *Atmos. Environ.* **1994**, *28* (6), 1089–1094. https://doi.org/10.1016/1352-2310(94)90286-0.

(43) Stutz, J.; Alicke, B.; Neftel, A. Nitrous Acid Formation in the Urban Atmosphere: Gradient Measurements of NO_2 and HONO over Grass in Milan, Italy. *J. Geophys. Res. Atmos.* **2002**, *107* (22), 8192. https://doi.org/10.1029/2001JD000390.

(44) Alicke, B., A. Geyer, A. Hofzumahaus, F. Holland, S. Konrad, H. W. Pätz, J. Schäfer, J. Stutz, A. Volz-Thomas, U. Platt. OH Formation by HONO Photolysis during the BERLIOZ Experiment. *J. Geophys. Res. Atmos.* **2003**, *108* (D4), 8247. https://doi.org/10.1029/2001JD000579.

(45) Zhang, J.; An, J.; Qu, Y.; Liu, X.; Chen, Y. Impacts of Potential HONO Sources on the Concentrations of Oxidants and Secondary Organic Aerosols in the Beijing-Tianjin-Hebei Region of China. *Sci. Total Environ.* **2019**, *647*, 836–852.

https://doi.org/10.1016/j.scitotenv.2018.08.030.

(46) Wang, T.; Xue, L.; Brimblecombe, P.; Lam, Y. F.; Li, L.; Zhang, L. Ozone Pollution in China: A Review of Concentrations, Meteorological Influences, Chemical Precursors, and Effects. *Sci. Total Environ.* **2017**, *575*, 1582–1596. https://doi.org/10.1016/j.scitotenv.2016.10.081.

(47) Sun, L.; Xue, L.; Wang, T.; Gao, J.; Ding, A.; Cooper, O. R.; Lin, M.; Xu, P.; Wang, Z.; Wang, X.; Wen, L.; Zhu, Y.; Chen, T.; Yang, L.; Wang, Y.; Chen, J.; Wang, W. Significant Increase of Summertime Ozone at Mount Tai in Central Eastern China. *Atmos. Chem. Phys.* **2016**, *16* (16), 10637–10650. https://doi.org/10.5194/acp-16-10637-2016.

TOC art